


Thermalization of open quantum systems using the multiple-Davydov-D₂ variational approach

Mantas Jakučionis  and Darius Abramavičius*Institute of Chemical Physics, Vilnius University, Sauletekio Avenue 9-III, 10222 Vilnius, Lithuania* (Received 3 March 2023; accepted 31 May 2023; published 8 June 2023)

Numerical implementation of an explicit phonon bath requires a large number of oscillator modes in order to maintain oscillators at the initial temperature when modeling energy relaxation processes. An additional thermalization algorithm may be useful in controlling the local temperature. In this paper we extend our previously proposed thermalization algorithm [M. Jakučionis and D. Abramavičius, *Phys. Rev. A* **103**, 032202 (2021)] to be used with the numerically exact multiple-Davydov-D₂ trial wave function for simulation of relaxation dynamics and spectroscopic signals of open quantum systems using the time-dependent Dirac-Frenkel variational principle. By applying it to the molecular aggregate model, we demonstrate how the thermalization approach significantly reduces the numerical cost of simulations by decreasing the number of oscillators needed to explicitly simulate the aggregate's environment fluctuations while maintaining correspondence to the exact population relaxation dynamics. Additionally, we show how the thermalization can be used to find the equilibrium state of the excited molecular aggregate, which is necessary for simulation of the fluorescence and other spectroscopic signals. The thermalization algorithm we present offers the possibility to investigate larger system-bath models than was previously possible using the multiple-Davydov-D₂ trial wave function and local heating effects in molecular complexes.

DOI: [10.1103/PhysRevA.107.062205](https://doi.org/10.1103/PhysRevA.107.062205)

I. INTRODUCTION

Open-quantum-system models are widely used to describe properties of molecular aggregates [1,2]. The system usually consists of molecular electronic states. Intramolecular vibrational degrees of freedom (DOFs), which play a major role in the relaxation process of the systems of interest, can also be included in the quantum-system model. The rest of the DOFs are treated as an environment of a constant temperature: the bath. The bath is modeled as a collection of quantum harmonic oscillators (QHOs) and is characterized by a continuous-fluctuation spectral density function [2–5]. Separation into the system and the bath parts is mostly a formality as the system-bath coupling has to be included to account for molecular environment-induced decoherence and temperature effects; hence the quantum dynamics penetrates into the bath and the bath also changes its state.

When using wave-function-based simulation approaches, it can be challenging to maintain a precise representation of the bath as a constant temperature thermostat, because energy exchange between the system and the bath can alter thermal properties of the bath. Generally, a large number of explicitly modeled QHO modes have to be included to minimize the negative effects of thermal energy accumulation in the bath, but this is numerically expensive. Therefore, one always has to balance between the size of the model, the accuracy of the chosen numerical method, and the method's numerical cost. Alternatively, one could numerically change the wave-function variables during its time evolution in a way so as to prevent accumulation of the thermal energy in the bath and to maintain it at a desired temperature, i.e., perform thermalization.

It is challenging to accurately simulate the dynamics of quantum systems that exchange energy and (quasi)particles with their surroundings, i.e., of the open quantum systems [6,7], because the numerical cost needed to propagate the corresponding dynamical equations in time increases exponentially with the number of DOFs. The wave-function approach based on the multiple-Davydov-D₂ trial wave function (multiple-Davydov-D₂ *Ansatz*) [8–12], along with the time-dependent variational principle, has been shown to be an excellent tool for accurately simulating the dynamics of system-bath models [8,13–19] and spectroscopic signals [10,18–21]. Despite relying on an adaptive time-dependent state basis set, the problem of rapidly growing numerical costs remains.

In a previous study we proposed the thermalization algorithm [22] to be used with the Davydov-D₂ *Ansatz* [13,23–28], which restricts QHOs to their lowest uncertainty states: coherent states [29,30] with Gaussian wave packets in their coordinate-momentum phase space. We demonstrated how the thermalization algorithm regulates the temperature of the environment and enables the electronically excited molecular system to relax into its equilibrium state at a given temperature [31–33] even when using a reduced number of bath oscillators, which greatly reduces numerical costs. The characteristics of the resulting equilibrium state are essential for modeling fluorescence, excited-state emission, excited-state absorption, and other spectroscopic signals [1]. However, the Davydov-D₂ *Ansatz* is a crude approximation of the actual system-bath model eigenstates and thus is unable to completely capture electronic population relaxation dynamics [10].

Meanwhile, the system-bath dynamics obtained using the multiple-Davydov *Ansätze* is consistent with the results from

other state-of-the-art methods, such as hierarchical equations of motion [9–11], the quasiadiabatic path integral [14], and the multiconfiguration time-dependent Hartree method [15,34], even when the number of bath oscillators is large. Due to the more complicated wave-function structure of the multiple-Davydov-D₂ ansatz, straightforward application of the D₂ Ansatz thermalization algorithm is not possible. In this work we extend the thermalization algorithm for the multiple-Davydov-D₂ Ansatz by introducing an additional state projection algorithm and adopting the coarse-grained scattering approximation.

In Sec. II we describe the thermalization algorithm for the multiple-Davydov-D₂ Ansatz. In Sec. III we provide a theoretical description of its application to simulating the fluorescence spectra. In Sec. IV we demonstrate its capabilities by simulating the excitation relaxation dynamics of an H-type molecular aggregate and its fluorescence spectrum. In Sec. V we discuss changes made to adapt the thermalization algorithm of the D₂ Ansatz for the multiple-Davydov-D₂ Ansatz.

II. THERMALIZATION OF THE MULTIPLE-DAVYDOV-D₂ ANSATZ

We consider a molecular aggregate model, where each molecule $n = 1, 2, \dots, N$ couples to its own local reservoir $k = 1, 2, \dots, N$, each of which consists of $q = 1, 2, \dots, Q$ QHO modes. The model is given by the Hamiltonian $\hat{H} = \hat{H}_S + \hat{H}_B + \hat{H}_{SB}$ with the system, the bath, and the system-bath coupling terms defined as

$$\hat{H}_S = \sum_n^N \varepsilon_n \hat{a}_n^\dagger \hat{a}_n + \sum_{n,m}^{n \neq m} J_{nm} \hat{a}_n^\dagger \hat{a}_m, \quad (1)$$

$$\hat{H}_B = \sum_{k,q}^{N,Q} \omega_{kq} \hat{b}_{kq}^\dagger \hat{b}_{kq}, \quad (2)$$

$$\hat{H}_{SB} = - \sum_n^N \hat{a}_n^\dagger \hat{a}_n \sum_q^Q \omega_{nq} g_{nq} (\hat{b}_{nq}^\dagger + \hat{b}_{nq}), \quad (3)$$

with the reduced Planck's constant set to $\hbar = 1$. Here ε_n is the n th molecule electronic excitation energy, J_{nm} denotes the resonant coupling between the n th and m th molecules, ω_{nq} denotes the frequency of the q th QHO in the k th local reservoir, and g_{nq} is the coupling strength between the q th oscillator in the n th local reservoir and the n th molecule. The operators \hat{a}_n^\dagger and \hat{a}_n represent the creation and annihilation operators for electronic excitations, respectively, while \hat{b}_{nq}^\dagger and \hat{b}_{nq} represent the creation and annihilation bosonic operators for QHOs.

In addition, we implicitly couple the system-bath model to the secondary bath characterized by a fixed temperature T . The coupling between the secondary and primary baths occurs via the scattering events that allow the system-bath model to exchange energy with the secondary bath and thermalize local reservoirs, as is described below.

The state of the system-bath model is given by the multiple-Davydov-D₂ wave function

$$|\Psi(t)\rangle = \sum_{i,n}^{M,N} \alpha_{i,n}(t) |n\rangle \otimes |\lambda_i(t)\rangle, \quad (4)$$

where $\alpha_{i,n}(t)$ is the i th multiple complex amplitude associated with a singly excited electronic state $|n\rangle$ localized on the n th molecule, $|n\rangle = \hat{a}_n^\dagger |0\rangle_{\text{el}}$. Here $|0\rangle_{\text{el}}$ is the electronic ground state. The complexity and accuracy of the multiple-Davydov-D₂ Ansatz can be adjusted by varying the multiplicity number M . The states of the QHO modes are represented by multidimensional coherent states

$$|\lambda_i(t)\rangle = \exp \sum_{k,q}^{N,Q} [\lambda_{i,kq}(t) \hat{b}_{kq}^\dagger - \lambda_{i,kq}^*(t) \hat{b}_{kq}] |0\rangle_{\text{vib}}, \quad (5)$$

where $\lambda_{i,kq}(t)$ is the i th multiple complex displacement parameter and $|0\rangle_{\text{vib}} = \otimes_{k,q} |0\rangle_{k,q}$ is the global vibrational ground state of all QHOs.

The multiple-Davydov-D₂ wave function describes a state of the system-bath model as a superposition of M multidimensional coherent state terms, which allows it to represent a wide range of system-bath model states beyond the Born-Oppenheimer and Gaussian approximations. The thermalization algorithm for the multiple-Davydov-D₂ Ansatz is realized by stochastic scattering events [35,36] during time evolution of the wave function. These events change the momenta p_{kq} of all the q th QHO modes of the k th local reservoir at once. We assume that the scattering probability $P_k(\theta, \tau_{\text{sc}})$ of θ scattering events occurring per time interval τ_{sc} with a scattering rate ν_k is given by a Poisson distribution

$$P_k(\theta, \tau_{\text{sc}}) = \frac{1}{\theta!} (\tau_{\text{sc}} \nu_k)^\theta e^{-\tau_{\text{sc}} \nu_k}. \quad (6)$$

Numerically, Poisson statistics are realized by simulating Bernoulli processes [37,38] in the limit of $\tau_{\text{sc}} \rightarrow 0$ while maintaining the condition that $\nu_k \tau_{\text{sc}} \ll 1$. To simulate the scattering events, we divide wave-function propagation into equal time length τ_{sc} intervals

$$t_i = (i\tau_{\text{sc}}, (i+1)\tau_{\text{sc}}], \quad i = 0, 1, \dots \quad (7)$$

At the end of each interval, for each local reservoir, we flip a biased coin with the probability $\nu_k \tau_{\text{sc}}$ of landing heads for all local reservoirs. If the k th coin lands heads, we change the momenta of all oscillator modes of that k th reservoir; otherwise, no changes are made. A list of scattering moments at which the numerical simulation is paused to perform the scatterings can be precomputed prior to starting the simulation by drawing probabilities for all local reservoir and all time intervals t_i from Eq. (6).

We assume that during the scattering event the local bath, which experiences the scattering, acquires thermal-equilibrium kinetic energy. Such a state is given by a single coherent state for one specific QHO. In order to set the new momentum values of the scattered reservoir oscillator modes, we first project the multiple-Davydov-D₂ wave function of Eq. (4) to its single-multiple Davydov-D₂ form

$$|\psi(t)\rangle = \sum_n^N \beta_n(t) |n\rangle \otimes |\tilde{\lambda}(t)\rangle, \quad (8)$$

where β_n are the projected complex electronic amplitudes and $|\tilde{\lambda}(t)\rangle$ is the projected multidimensional coherent state, which is defined later. This follows the decoherence idea [39], where the macroscopic environment performs a collapse of

the wave function into a set of preferred states, in our case, the electronic-vibrational states $|n\rangle \otimes |\tilde{\lambda}(t)\rangle$. The projected complex electronic amplitudes are equal to

$$\beta_n(t) = \sum_i^M \alpha_{i,n}(t) \langle \tilde{\lambda}(t) | \lambda_i(t) \rangle, \quad (9)$$

while the projected multidimensional coherent state

$$|\tilde{\lambda}(t)\rangle = \exp \sum_{k,q}^{N,Q} [\tilde{\lambda}_{kq}(t) \hat{b}_{kq}^\dagger - \tilde{\lambda}_{kq}^*(t) \hat{b}_{kq}] |0\rangle_{\text{vib}} \quad (10)$$

is defined in terms of the complex displacements

$$\tilde{\lambda}_{kq}(t) = \frac{1}{\sqrt{2}} [x_{kq}(t) + ip_{kq}(t)], \quad (11)$$

where $x_{kq}(t)$ and $p_{kq}(t)$ are QHO coordinate and momentum expectation values

$$x_{kq} = \frac{1}{\sqrt{2}} \sum_{i,j,n}^{M,M,N} \alpha_{i,n}^* \alpha_{j,n} \langle \lambda_i | \lambda_j \rangle \sum_{k,q}^{N,Q} (\lambda_{i,kq}^* + \lambda_{j,kq}), \quad (12)$$

$$p_{kq} = \frac{i}{\sqrt{2}} \sum_{i,j,n}^{M,M,N} \alpha_{i,n}^* \alpha_{j,n} \langle \lambda_i | \lambda_j \rangle \sum_{k,q}^{N,Q} (\lambda_{i,kq}^* - \lambda_{j,kq}) \quad (13)$$

calculated from the multiple-Davydov-D₂ Ansatz, where $\langle \lambda_i | \lambda_j \rangle$ is the overlap of two coherent states

$$\langle \lambda_i | \lambda_j \rangle = \exp \sum_{k,q}^{N,Q} \left[\lambda_{i,kq}^* \lambda_{j,kq} - \frac{1}{2} (|\lambda_{i,kq}|^2 + |\lambda_{j,kq}|^2) \right]. \quad (14)$$

This completes the projection operation of the multiple-Davydov-D₂ state, given by Eq. (4), into its simplified D₂ form in Eq. (8).

Once the projected wave function is deduced, we modify the momenta of the scattered oscillators by sampling the QHO diagonal density operator distribution in the coherent state representation at temperature T , known as the Glauber-Sudarshan distribution [14,40–42]

$$\mathcal{P}(\tilde{\lambda}_{kq}) = \mathcal{Z}_{kq}^{-1} \exp[-|\tilde{\lambda}_{kq}|^2 (e^{\omega_{kq}/k_B T} - 1)]. \quad (15)$$

For scattered modes, we set the momentum values in Eq. (11) to

$$p_{kq}(t) = \sqrt{2} \text{Im}(\tilde{\lambda}_{kq}^{\mathcal{P}}), \quad (16)$$

where $\tilde{\lambda}_{kq}^{\mathcal{P}}$ is a sample drawn from the Glauber-Sudarshan distribution. In addition, \mathcal{Z}_{kq}^{-1} and ω_{kq} are partition functions and frequencies of the QHO, respectively, and k_B is the Boltzmann constant. During the scattering events, coordinates x_{kq} of both the scattered and nonscattered modes remain unchanged. Notice that the local baths, which do not experience scattering, remain unaffected by the scattering of other modes.

Now that the wave function of the system-bath model after scattering is known [given by Eq. (8)] we rewrite it in the multiple-Davydov-D₂ wave-function form of Eq. (4) by populating amplitudes and displacements of the first multiple

$i = 1$ as

$$\alpha_{1,n}(t) = \beta_n(t), \quad (17)$$

$$\lambda_{1,kq}(t) = \tilde{\lambda}_{kq}(t). \quad (18)$$

The amplitudes of the unpopulated multiples are set to $\alpha_{j=2,\dots,M,n}(t) = 0$, while the unpopulated displacements are positioned in a layered hexagonal pattern around the populated coherent state [18]

$$\lambda_{j=2,\dots,M,kq}(t) = \lambda_{1,kq}(\tau) + \frac{1}{4} [1 + \lfloor \beta(j) \rfloor] e^{i2\pi[\beta(j)+(1/12)\lfloor \beta(j) \rfloor]}, \quad (19)$$

where $\beta(j) = (j-2)/6$ is the coordination function and $\lfloor x \rfloor$ is the floor function. The exact arrangement of displacements of the unpopulated multiples is not critical as long as the distance in the phase space to the populated multiple coherent state is not too large; otherwise, the initially unpopulated multiples will not contribute to further dynamics [16,43].

Once the scattered multiple-Davydov-D₂ wave function is determined and the scattering event is finalized, further simulation of multiple-Davydov-D₂ dynamics according to equations of motion (EOMs) proceeds. This procedure generates a stochastic wave-function trajectory, where the system-bath model at each time moment is described by a pure state, which is a single member of a statistical ensemble [14,41]. The thermalized model dynamics is obtained by averaging observables over an ensemble of wave-function trajectories γ , which differ by their initial amplitudes $\alpha_{i,n}(0)$, initial coherent state displacements $\lambda_{i,kq}(0)$, and a sequence of scattering events. Ensemble averaging is performed in a parallelized Monte Carlo scheme.

III. THERMALIZED FLUORESCENCE SPECTRA

Wave-function trajectories allow calculation of an arbitrary observable. Calculation of the equilibrium fluorescence spectrum requires us to know the thermally equilibrated state of the excited model. The presented thermalization procedure allows us to obtain such a state and calculate the fluorescence spectrum.

In general, the frequency-domain spectrum of a quantum system can be written as a Fourier transform

$$F(\omega) = \text{Re} \int_0^\infty dt e^{i\omega t} S(t) \quad (20)$$

of the corresponding time-domain response function $S(t)$. The fluorescence response function $S_{\text{fl}}(t)$ is a specific case of the more general time-resolved fluorescence (TRF) response function [1,44]

$$S_{\text{TRF}}(\tau_{\text{eq}}, t) = \frac{1}{\Gamma} \sum_{\gamma=1}^{\Gamma} \langle \Psi_{\text{G}}(0) |_{\gamma} \hat{\mu}_- \hat{\mathcal{V}}_{\text{E}}^\dagger(\tau_{\text{eq}} + t) \hat{\mu}_+ \times \hat{\mathcal{V}}_{\text{G}}(t) \hat{\mu}_- \hat{\mathcal{V}}_{\text{E}}(\tau_{\text{eq}}) \hat{\mu}_+ | \Psi_{\text{G}}(0) \rangle_{\gamma}, \quad (21)$$

where $\hat{\mathcal{V}}_{\text{E}}$ and $\hat{\mathcal{V}}_{\text{G}}$ are the excited- and ground-state system-bath propagators

$$\hat{\mathcal{V}}_{\text{A}}(t_1) | \Psi_{\text{A}}(t_2) \rangle = | \Psi_{\text{A}}(t_1 + t_2) \rangle, \quad (22)$$

$\hat{\mu}_+ = \sum_n^N (\mathbf{e} \cdot \boldsymbol{\mu}_n) \hat{a}_n^\dagger$ and $\hat{\mu}_- = \sum_n^N (\mathbf{e} \cdot \boldsymbol{\mu}_n) \hat{a}_n$ are the excitation creation and annihilation operators of the system [18], respectively, $\boldsymbol{\mu}_n$ is the electronic transition dipole moment vector, \mathbf{e} is the external field polarization vector, and $|\Psi_G(0)\rangle_\gamma$ is a model ground state with an initial condition of the γ th trajectory. The EOMs for propagating the multiple-Davydov-D₂ wave function, as well as the approach to solving them, are described in detail in Refs. [18,43].

Here $S_{\text{TRF}}(\tau_{\text{eq}}, t)$ is a function of two times: the equilibration time τ_{eq} and the coherence time t . During the equilibration time, the system evolves in its excited state and, due to the system-bath interaction, relaxes to an equilibrium state. After this, during the coherence time, spontaneous emission occurs.

We will apply thermalization during the equilibration time to facilitate the relaxation of the system-bath model into the lowest-energy equilibrium state by removing excess thermal energy from local reservoirs. We denote by $\hat{G}_{E,\gamma}$ the excited-state propagator \hat{Y}_E but with thermalization. Then the thermalized TRF (TTRF) response function can be written as

$$\tilde{S}_{\text{TRF}}(\tau_{\text{eq}}, t) = \frac{1}{\Gamma} \sum_{\gamma=1}^{\Gamma} \langle \Psi_G(0) |_\gamma \hat{\mu}_- \hat{G}_{E,\gamma}^\dagger(\tau_{\text{eq}}) \hat{Y}_G^\dagger(t) \hat{\mu}_+ \times \hat{Y}_G(t) \hat{\mu}_- \hat{G}_{E,\gamma}(\tau_{\text{eq}}) \hat{\mu}_+ | \Psi_G(0) \rangle_\gamma. \quad (23)$$

By considering the equilibration time to be long enough to reach the equilibrium state of the system-bath model, we define the fluorescence response function as

$$S_{\text{fl}}(t) = \lim_{\tau_{\text{eq}} \rightarrow \infty} S_{\text{TRF}}(\tau_{\text{eq}}, t) \quad (24)$$

and the thermalized fluorescence (TF) response function as

$$\tilde{S}_{\text{fl}}(t) = \lim_{\tau_{\text{eq}} \rightarrow \infty} \tilde{S}_{\text{TRF}}(\tau_{\text{eq}}, t). \quad (25)$$

The spectra obtained using the fluorescence response function without and with thermalization will be compared in the next section. For the numerical simulation, the required equilibration time interval has to be deduced by increasing τ_{eq} until the resulting fluorescence spectra converge.

IV. RESULTS

To investigate the thermalization algorithm for the multiple-Davydov-D₂ *Ansatz*, we will analyze the linear trimer model, which we previously used to study thermalization of the Davydov-D₂ *Ansatz* [22]. The model consists of $N = 3$ coupled molecules, with excited-state energies ε_n being equal to 0, 250, and 500 cm^{-1} , forming an energy funnel. The nearest-neighbor couplings are set to $J_{1,2} = J_{2,3} = 100 \text{ cm}^{-1}$ and $J_{3,1} = 0$. The electronic dipole moment vectors of molecules are $\boldsymbol{\mu}_n = (1, 0, 0)$ in the Cartesian coordinate system. This classifies the trimer as the H-type molecular aggregate [45].

The QHOs of local molecular reservoirs are characterized by the super-Ohmic [46] spectral density function $C''(\omega) = \omega(\omega/\omega_c)^{s-1} \exp(-\omega/\omega_c)$ with an order parameter $s = 2$ and a cutoff frequency $\omega_c = 100 \text{ cm}^{-1}$. The QHO frequencies are $\omega_{kq} = \omega_0 + (q-1)\Delta\omega$, where the frequency offset is $\omega_0 = 0.01 \text{ cm}^{-1}$. The reorganization energy of

each local reservoir is $\Lambda_k = \sum_q \omega_{kq} g_{kq}^2 = 100 \text{ cm}^{-1}$. The scattering time step size is set to $\tau_{\text{sc}} = 0.01 \text{ ps}$. Finally, the ensemble consists of 900 wave-functions trajectories, which we found to be sufficient to obtain the converged model dynamics. The multiple-Davydov-D₂ *Ansatz* multiplicity $M = 5$ is used as the results with a higher multiplicity quantitatively match the $M = 5$ case.

We will be considering three bath models: the dense bath model, where the spectral density function $C''(\omega)$ is discretized into $Q = 75$ oscillators per local reservoir with a step size of $\Delta\omega = 10 \text{ cm}^{-1}$; the sparse bath model, where the number of modes is reduced by a factor of 5 to just $Q = 15$ oscillators per local reservoir with $\Delta\omega = 50 \text{ cm}^{-1}$; and the sparse bath with thermalization model, where $C''(\omega)$ is discretized according to the sparse bath model and thermalization is used.

In the absence of the bath, the system has three single-excitation stationary exciton states with energies $E_1^{\text{exc}} \approx -37.23 \text{ cm}^{-1}$, $E_2^{\text{exc}} = 250 \text{ cm}^{-1}$, and $E_3^{\text{exc}} \approx 537.23 \text{ cm}^{-1}$, satisfying the time-independent Schrödinger equation

$$\hat{H}_S \Phi_n^{\text{exc}} = E_n^{\text{exc}} \Phi_n^{\text{exc}}, \quad (26)$$

with the system Hamiltonian given by Eq. (1). The exciton eigenstates [2,4] Φ_n^{exc} have their excitations delocalized over multiple molecules [41]. Therefore, it is convenient to analyze molecular aggregate excitation relaxation dynamics in terms of excitons as they are natural quasiparticles of the aggregate. We define the probability of finding the aggregate in its n th excitonic state as the population, given by

$$\rho_n^{\text{exc}}(t) = \sum_{k,l,i,j} (\Phi_k^{\text{exc}})_n^* \langle \alpha_{i,k}^*(t) \alpha_{j,l}(t) S_{i,j}(t) \rangle_{\text{th}} (\Phi_l^{\text{exc}})_n, \quad (27)$$

where $\langle \dots \rangle_{\text{th}}$ is the averaging over an ensemble of wave-function trajectories. Using the multiple-Davydov-D₂ *Ansatz*, we proceed with the following analysis.

First, we study the electronic excitation dynamics. The initial excitonic-state populations correspond to the optically excited highest-energy states $\rho_3^{\text{exc}} = 1$ and $\rho_{1,2}^{\text{exc}} = 0$, while the initial QHO displacements $\lambda_{i,kq}(0)$ are sampled from the Glauber-Sudarshan distribution in Eq. (15) to account for the initial temperatures of $T_k = 77 \text{ K}$.

In Fig. 1 we display the trimer model exciton-state populations $\rho_n^{\text{exc}}(t)$ and average temperatures [47] $T_k(t)$ of local reservoirs for all three bath models. The aggregate environment causes dephasing between excitonic states and induces irreversible population relaxation [1,2]. The population dynamics of the dense bath models exhibits a sequential relaxation from the initially populated highest-energy excitonic state to the lowest-energy state via the intermediate state. Eventually, the population distribution reaches the equilibrium state. The majority of the excitation energy is transferred to oscillators of local reservoirs. We observe an increase of temperatures [47–49] due to the finite number of oscillators in local reservoirs. An infinite number of oscillators would have to be included to maintain a constant temperature at the initial value. The initial rapid rise in temperature is due to oscillator reorganization in the aggregate's electronic excited-state manifold, while the following slow rise is due to energy transfer from the system to local reservoirs.

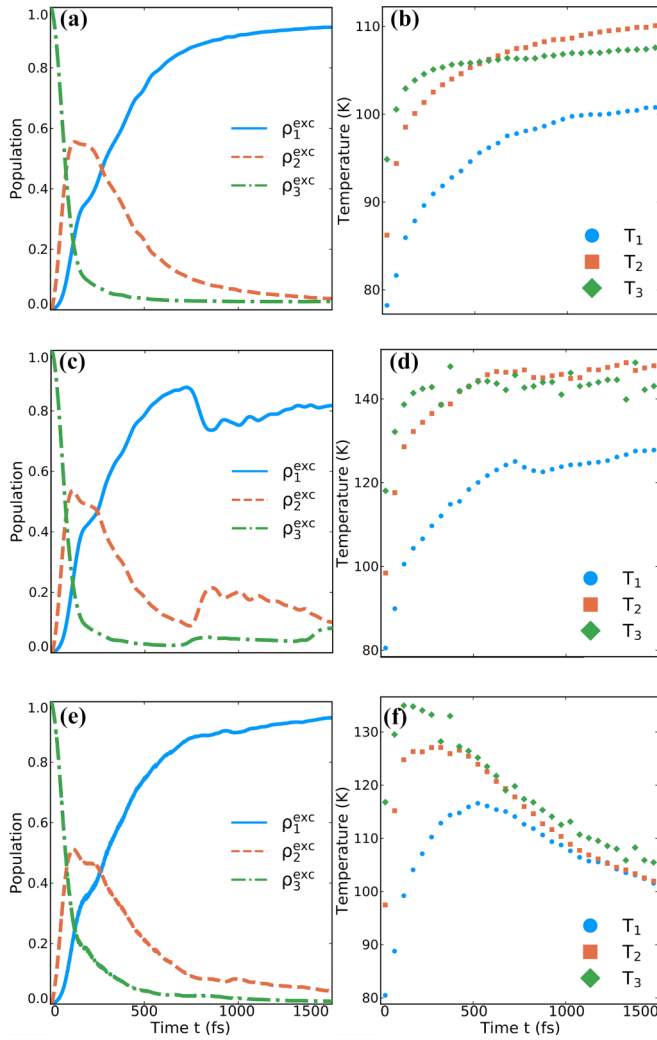


FIG. 1. Exciton-state populations $\rho_i^{\text{exc}}(t)$ and the average temperatures $T_k(t)$ of local reservoirs of the trimer in (a) and (b) the dense bath model, (c) and (d) the sparse bath model, and (e) and (f) the sparse bath model with thermalization.

In the sparse bath model, we observe that if the number of vibrational modes is reduced, the population dynamics become skewed due to an insufficiently dense representation of the spectral density function. Furthermore, the temperature increase is higher than that for the dense bath model, which further changes the characteristics of the resulting equilibrium state.

When the thermalization algorithm is applied to the sparse bath model with a scattering rate $\nu_k = 1.25 \text{ ps}^{-1}$, the population dynamics is restored and qualitatively matches that of the dense model. Although the initial temperatures of the local reservoirs exceed those of the dense bath model, they gradually decrease due to thermalization, and this rate can be adjusted by changing the scattering rate.

Next we turn our attention to simulating the fluorescence spectrum of the linear trimer with the dense bath model with scattering rate $\nu_k = 1 \text{ ps}^{-1}$. The initial excitonic-state population distribution is now calculated in terms of the system-field interaction, as described in Ref. [18].

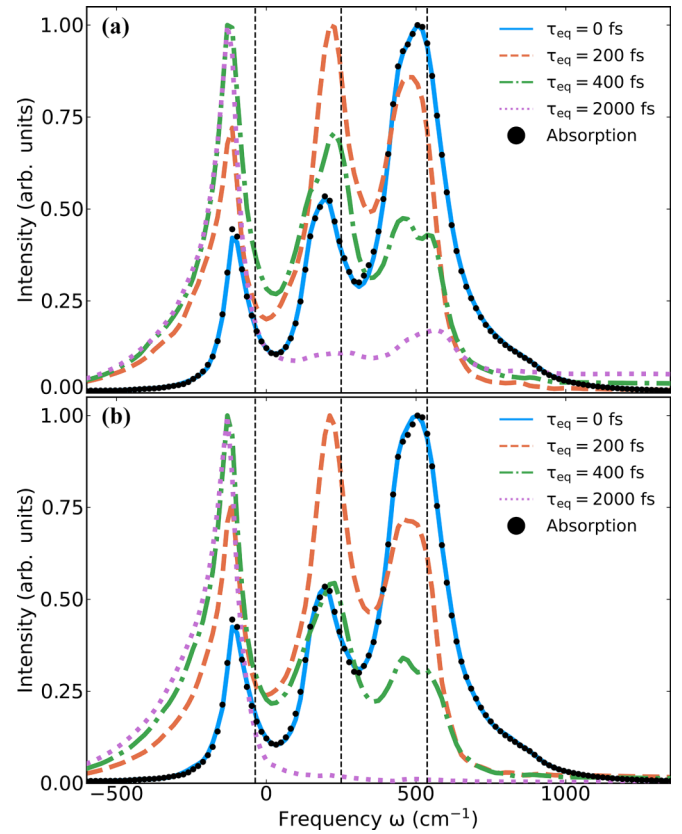


FIG. 2. The (a) TRF and (b) TTRF spectra of the trimer in the dense bath model, simulated with increasing equilibration time τ_{eq} . The absorption spectrum is also shown. Vertical dashed lines show energies E^{exc} of the excitonic states.

In Fig. 2 we compare the TRF and TTRF spectra with increasing equilibration times τ_{eq} . When $\tau_{\text{eq}} = 0$, both the TRF and TTRF spectra are equivalent and exactly match the absorption spectrum, which consists of three peaks due to a transition involving the combined excitonic-vibronic (vibronic) states and cannot be regarded as purely excitonic. For reference, vertical dotted lines indicate energies E^{exc} of excitonic states. These do not match the three peak energies exactly due to the system being coupled to the environment.

By allowing equilibration to occur, $\tau_{\text{eq}} > 0$, both the TRF and TTRF spectra show a peak intensity shift towards lower energies as excitation relaxes towards the equilibrated state during the equilibration time. After equilibrating for $\tau_{\text{eq}} = 2 \text{ ps}$, we find that both spectra have converged and do not change with longer τ_{eq} . Therefore, the TRF and TTRF spectra at $\tau_{\text{eq}} = 2 \text{ ps}$ can be considered as the fluorescence and TF spectra of the trimer model as defined in Eqs. (24) and (25).

Both spectra exhibit their highest intensities at the energies of the lowest vibronic states. However, the fluorescence spectrum also has considerable intensities at energies of the intermediate and highest vibronic states. Surprisingly, the higher-energy peak is more intense than the intermediate peak. The TF spectrum intensities at these energies are negligible, which indicates that the thermalization allows the trimer model to reach a lower-energy equilibrium state, which is not

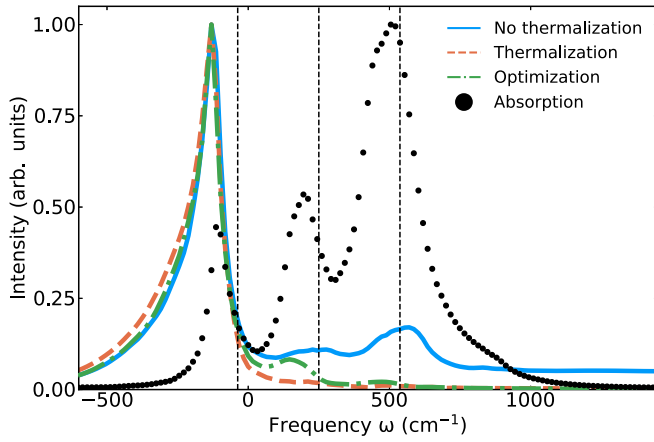


FIG. 3. Comparison of the fluorescence spectra of the trimer with the dense bath model obtained without thermalization, with thermalization, and using the optimization approach. The equilibration time is $\tau_{\text{eq}} = 2$ ps. The absorption spectrum is also shown. Vertical dashed lines show energies E^{exc} of the excitonic states.

longer hindered by the excess thermal energy accumulation in QHOs of local reservoirs.

In Fig. 3 we also compare the obtained fluorescence and TF spectra with the fluorescence spectrum simulated using a previously proposed excited-state numerical optimization approach [19,50,51]. It relies on finding the model's lowest-energy excitonic state in terms of the multiple-Davydov- D_2 Ansatz parameters and then applying thermal fluctuations to effectively generate the model in a lowest-energy equilibrium state at a temperature of 77 K. We see that all three methods produce a similar lowest vibronic peak, but the TF spectrum has a higher-intensity tail towards the low-energy side and almost no intensities at energies of the intermediate and the highest vibronic states, while the fluorescence spectrum simulated using the optimization approach has a low intensity at the energy of the intermediate vibronic states. The optimization approach spectrum more closely resembles that of the thermalized model than the nonthermalized spectrum.

V. DISCUSSION

Starting from an arbitrary nonequilibrium initial condition, a closed quantum system will not equilibrate due to energy conservation. The thermalization procedure is necessary to guarantee proper thermal equilibrium in the long run for all bath oscillators. This requires introducing the concept of primary and secondary baths. In our model the primary bath is a part of explicit quantum DOFs, while the secondary bath is a thermal reservoir with infinite thermal capacity, i.e., it maintains a constant temperature in any energy exchange process. In this case, the secondary bath cannot be described by mechanical equations; only statistical or thermodynamical concepts apply. Our statistical algorithm performs energy exchange between the primary and secondary baths using the statistical scattering idea: The primary bath state is reset to the thermally equilibrated state, thus giving up excess energy to or drawing additional energy from the secondary bath. This is a major extension of the explicit quantum time-dependent

variational principle (TDVP) theory: The extended model covers a broader range of phenomena, i.e., local heating and cooling, as well as bath oscillator dynamic localization, which are not available in the standard TDVP theory.

In order to adapt the Davydov- D_2 Ansatz thermalization algorithm for the multiple-Davydov- D_2 Ansatz, several extensions were made. During the time evolution of the system-bath model, the multiple-Davydov- D_2 Ansatz multiples become correlated, leading to a non-Gaussian bath wave function. It becomes impossible to represent a new Gaussian wave function of scattered QHO modes, sampled from Eq. (15), without changing the wave function of the rest of the nonscattered oscillators at the same time. Therefore, we chose to project the multiple-Davydov- D_2 Ansatz into the Davydov- D_2 Ansatz whenever scattering occurred, allowing us to correctly represent the newly sampled Gaussian wave function of scattered oscillators. This idea requires consideration of a few aspects.

The projected Davydov- D_2 wave function accurately maintains average coordinates and momenta of the multiple-Davydov- D_2 Ansatz QHO states, while variances and higher-order moments are affected. This causes variation of excitation relaxation dynamics compared to the standard multiple-Davydov- D_2 Ansatz. However, system-bath models mostly rely only on the linear coupling between the system and average coordinates of QHO modes; therefore, as seen in Fig. 1, the discrepancy is minimal. The higher-order couplings become necessary when anharmonic vibrational modes or changes to their frequencies upon excitation are considered [19,52].

To maintain the close correspondence to the standard multiple-Davydov- D_2 Ansatz, the projection should not occur too often. This is because, after scattering, it takes time for the wave function to again become correlated between its many multiples, i.e., to take advantage of the unpopulated multiple-Davydov- D_2 Ansatz multiples after projection. If the repopulation time is shorter than the time between projection operations, the model population dynamics becomes similar to that of the Davydov- D_2 Ansatz, even though the multiple-Davydov- D_2 Ansatz is being used. The average time interval between projection operations is determined by the scattering rate ν_k , a property of the physical system, while the scattering time τ_{sc} is a parameter of the model and must be as small as necessary to ensure the Bernoulli-to-Poisson statistics transition condition $\nu_k \tau_{\text{sc}} \ll 1$.

To increase the average time between projection operations, we adopt a coarser scattering approach for the multiple-Davydov- D_2 Ansatz compared to the Davydov- D_2 Ansatz. Instead of considering scattering events of individual oscillators, we consider events where all oscillators of certain local reservoirs are scattered at once, requiring only a single projection operation to scatter many oscillators at once. This approach allows the multiple-Davydov- D_2 Ansatz to continue utilizing all its multiples for the improved accuracy over the Davydov- D_2 Ansatz while reducing the number of explicitly modeled oscillators needed to maintain the local reservoirs' temperatures close to initial values, thereby reducing the numerical cost.

Using the multiple-Davydov- D_2 Ansatz to simulate the population dynamics of the trimer model, it took an average of 166 min per trajectory using the dense bath model, but

only 1.3 min using the sparse bath model and 2 min using the sparse bath model with thermalization. The computational overhead of thermalization is small compared to the overall time savings when switching from using the dense bath to the sparse bath. The numerical cost reduction is also greater for the multiple-Davydov- D_2 Ansatz than for the Davydov- D_2 Ansatz in Ref. [22], because the multiple-Davydov- D_2 Ansatz EOMs constitute an implicit system of differential equations, which require a more involved two-step numerical approach to find a solution [18,43]. By considering fewer oscillators in each local reservoir, simulations of the dynamics and spectroscopic signals of aggregates made up of more molecules become possible.

Computing a single trajectory of the TTRF response function in Eq. (23) with an equilibration time of $\tau_{\text{eq}} = 2$ ps took an average of 79 min. The previously proposed optimization method [19] for simulating fluorescence spectra does not require propagation during the equilibration time interval of the TRF response function and has to be computed only once, but it takes 193 min. In general, we find that the computation of TTRF is more reliable and numerically stable. The optimization approach struggles to consistently find the lowest-energy excitonic state of the model due to its heuristic nature, requiring many attempts to find the solution and eventually having to choose the lowest-energy one. This is particularly apparent when a wide range of oscillator frequencies are included.

For elementary system-bath models without Hamiltonian parameter disorder, the optimization approach can be a

good starting point for fluorescence spectra simulation. However, a more accurate spectrum most likely will be obtained using the TTRF approach. For models with Hamiltonian disorder, e.g., static molecule excitation energy disorder [53–55], the optimization approach would require finding the model's lowest-energy excitonic state for each realization of the Hamiltonian, negating its advantage of having to perform the optimization procedure only once.

In conclusion, the thermalization algorithm presented for the numerically exact multiple-Davydov- D_2 Ansatz allows us to reduce the numerical cost of system-bath model simulations by having to explicitly include fewer bath oscillators while maintaining a correspondence with the exact relaxation dynamics. The thermalization algorithm efficiently controls molecular heating effects due to the reduced number of oscillators. Furthermore, the application of thermalization to the simulation of fluorescence spectra demonstrates a lower computation time, greater numerical stability, and higher accuracy compared to the numerical optimization approach.

ACKNOWLEDGMENTS

We thank the Research Council of Lithuania for financial support (Grant No. S-MIP-23-48). Computations were performed on resources at the High Performance Computing Center, HPC Sauletekis, of the Faculty of Physics, Vilnius University.

-
- [1] S. Mukamel, *Principles of Nonlinear Optical Spectroscopy* (Oxford University Press, Oxford, 1995).
- [2] L. Valkunas, D. Abramavičius, and T. Mančal, *Molecular Excitation Dynamics and Relaxation* (Wiley-VCH, Weinheim, 2013).
- [3] C. J. Bardeen, The structure and dynamics of molecular excitons, *Annu. Rev. Phys. Chem.* **65**, 127 (2014).
- [4] H. van Amerongen, R. van Grondelle, and L. Valkunas, *Photosynthetic Excitons* (World Scientific, Singapore, 2000).
- [5] M. Schröter, S. Ivanov, J. Schulze, S. Polyutov, Y. Yan, T. Pullerits, and O. Kühn, Exciton-vibrational coupling in the dynamics and spectroscopy of Frenkel excitons in molecular aggregates, *Phys. Rep.* **567**, 1 (2015).
- [6] H.-P. Breuer and F. Petruccione, *The Theory of Open Quantum Systems* (Oxford University Press, Oxford, 2007).
- [7] U. Weiss, *Quantum Dissipative Systems* (World Scientific, Singapore, 2012).
- [8] N. Zhou, Z. Huang, J. Zhu, V. Chernyak, and Y. Zhao, Polaron dynamics with a multitude of Davydov D_2 trial states, *J. Chem. Phys.* **143**, 014113 (2015).
- [9] L. Wang, L. Chen, N. Zhou, and Y. Zhao, Variational dynamics of the sub-Ohmic spin-boson model on the basis of multiple Davydov D_1 states, *J. Chem. Phys.* **144**, 024101 (2016).
- [10] N. Zhou, L. Chen, Z. Huang, K. Sun, Y. Tanimura, and Y. Zhao, Fast, Accurate simulation of polaron dynamics and multidimensional spectroscopy by multiple Davydov trial states, *J. Phys. Chem. A* **120**, 1562 (2016).
- [11] L. Chen, M. Gelin, and Y. Zhao, Dynamics of the spin-boson model: A comparison of the multiple Davydov D_1 , $D_{1.5}$, D_2 Ansätze, *Chem. Phys.* **515**, 108 (2018).
- [12] Y. Zhao, K. Sun, L. Chen, and M. Gelin, The hierarchy of Davydov's Ansätze and its applications, *WIREs Comput. Mol. Sci.* **12**, e1589 (2022).
- [13] Z. Huang, L. Chen, N. Zhou, and Y. Zhao, Transient dynamics of a one-dimensional Holstein polaron under the influence of an external electric field, *Ann. Phys. (Berlin)* **529**, 1600367 (2017).
- [14] L. Wang, Y. Fujihashi, L. Chen, and Y. Zhao, Finite-temperature time-dependent variation with multiple Davydov states, *J. Chem. Phys.* **146**, 124127 (2017).
- [15] L. Chen, M. F. Gelin, and W. Domcke, Multimode quantum dynamics with multiple Davydov D_2 trial states: Application to a 24-dimensional conical intersection model, *J. Chem. Phys.* **150**, 024101 (2019).
- [16] M. Jakučionis, T. Mančal, and D. Abramavičius, Modeling irreversible molecular internal conversion using the time-dependent variational approach with s D_2 ansatz, *Phys. Chem. Chem. Phys.* **22**, 8952 (2020).
- [17] L. Wang, F. Zheng, J. Wang, F. Großmann, and Y. Zhao, Schrödinger-cat states in Landau-Zener-Stückelberg-Majorana interferometry: A multiple Davydov Ansatz approach, *J. Phys. Chem. B* **125**, 3184 (2021).
- [18] M. Jakučionis, A. Žukas, and D. Abramavičius, Modeling molecular J and H aggregates using multiple-Davydov D_2 ansatz, *Phys. Chem. Chem. Phys.* **24**, 17665 (2022).
- [19] M. Jakučionis, A. Žukas, and D. Abramavičius, Inspecting molecular aggregate quadratic vibronic coupling effects using squeezed coherent states, *Phys. Chem. Chem. Phys.* **25**, 1705 (2023).
- [20] K. W. Sun, M. F. Gelin, V. Y. Chernyak, and Y. Zhao, Davydov Ansatz as an efficient tool for the simulation of nonlinear optical

- response of molecular aggregates, *J. Chem. Phys.* **142**, 212448 (2015).
- [21] Y. Zhao, The hierarchy of Davydov's Ansatz: From guesswork to numerically "exact" many-body wave functions, *J. Chem. Phys.* **158**, 080901 (2023).
- [22] M. Jakučionis and D. Abramavičius, Temperature-controlled open-quantum-system dynamics using a time-dependent variational method, *Phys. Rev. A* **103**, 032202 (2021).
- [23] J. Sun, B. Luo, and Y. Zhao, Dynamics of a one-dimensional Holstein polaron with the Davydov ansätze, *Phys. Rev. B* **82**, 014305 (2010).
- [24] B. Luo, J. Ye, C. Guan, and Y. Zhao, Validity of time-dependent trial states for the Holstein polaron, *Phys. Chem. Chem. Phys.* **12**, 15073 (2010).
- [25] M. Jakučionis, V. Chorošajev, and D. Abramavičius, Vibrational damping effects on electronic energy relaxation in molecular aggregates, *Chem. Phys.* **515**, 193 (2018).
- [26] M. Jakučionis, I. Gaiziunas, J. Sulskus, and D. Abramavičius, Simulation of ab initio optical absorption spectrum of β -carotene with fully resolved S_0 and S_2 vibrational normal modes, *J. Phys. Chem. A* **126**, 180 (2022).
- [27] A. S. Davydov, Solitons in molecular systems, *Phys. Scr.* **20**, 387 (1979).
- [28] A. C. Scott, Davydov's soliton revisited, *Physica D* **51**, 333 (1991).
- [29] W.-M. Zhang, D. H. Feng, and R. Gilmore, Coherent states: Theory and some applications, *Rev. Mod. Phys.* **62**, 867 (1990).
- [30] S. Kais and R. D. Levine, Coherent states for the Morse oscillator, *Phys. Rev. A* **41**, 2301 (1990).
- [31] J. M. Moix, Y. Zhao, and J. Cao, Equilibrium-reduced density matrix formulation: Influence of noise, disorder, and temperature on localization in excitonic systems, *Phys. Rev. B* **85**, 115412 (2012).
- [32] Y. Subaşı, C. H. Fleming, J. M. Taylor, and B. L. Hu, Equilibrium states of open quantum systems in the strong coupling regime, *Phys. Rev. E* **86**, 061132 (2012).
- [33] A. Gelzinis and L. Valkunas, Analytical derivation of equilibrium state for open quantum system, *J. Chem. Phys.* **152**, 051103 (2020).
- [34] J. Zeng and Y. Yao, Variational squeezed Davydov ansatz for realistic chemical systems with nonlinear vibronic coupling, *J. Chem. Theory Comput.* **18**, 1255 (2022).
- [35] M. B. Plenio and P. L. Knight, The quantum-jump approach to dissipative dynamics in quantum optics, *Rev. Mod. Phys.* **70**, 101 (1998).
- [36] K. Luoma, W. T. Strunz, and J. Piilo, Diffusive Limit of Non-Markovian Quantum Jumps, *Phys. Rev. Lett.* **125**, 150403 (2020).
- [37] V. N. Kampen, *Stochastic Processes in Physics and Chemistry* (Elsevier, Amsterdam, 2007).
- [38] D. P. Bertsekas and J. N. Tsitsiklis, *Introduction to Probability* (IOP, Bristol, 2008).
- [39] M. Schlosshauer, *Decoherence and the Quantum-To-Classical Transition* (Springer, Berlin, 2007).
- [40] R. J. Glauber, Coherent and incoherent states of the radiation field, *Phys. Rev.* **131**, 2766 (1963).
- [41] V. Chorošajev, O. Rancova, and D. Abramavičius, Polaronic effects at finite temperatures in the B850 ring of the LH2 complex, *Phys. Chem. Chem. Phys.* **18**, 7966 (2016).
- [42] Q. Xie, H. Zhong, M. T. Batchelor, and C. Lee, The quantum Rabi model: Solution and dynamics, *J. Phys. A: Math. Theor.* **50**, 113001 (2017).
- [43] M. Werther and F. Großmann, Apoptosis of moving nonorthogonal basis functions in many-particle quantum dynamics, *Phys. Rev. B* **101**, 174315 (2020).
- [44] V. Balevičius, Jr., L. Valkunas, and D. Abramavičius, Modeling of ultrafast time-resolved fluorescence applied to a weakly coupled chromophore pair, *J. Chem. Phys.* **143**, 074101 (2015).
- [45] N. J. Hestand and F. C. Spano, Expanded theory of H- and J-molecular aggregates: The effects of vibronic coupling and intermolecular charge transfer, *Chem. Rev.* **118**, 7069 (2018).
- [46] A. Kell, X. Feng, M. Reppert, and R. Jankowiak, On the shape of the phonon spectral density in photosynthetic complexes, *J. Phys. Chem. B* **117**, 7317 (2013).
- [47] D. Abramavičius, V. Chorošajev, and L. Valkunas, Tracing feed-back driven exciton dynamics in molecular aggregates, *Phys. Chem. Chem. Phys.* **20**, 121225 (2018).
- [48] V. Scarani, M. Ziman, P. Štelmachovič, N. Gisin, and V. Bužek, Thermalizing Quantum Machines: Dissipation and Entanglement, *Phys. Rev. Lett.* **88**, 097905 (2002).
- [49] A. W. Chin, J. Prior, R. Rosenbach, F. Caycedo-Soler, S. F. Huelga, and M. B. Plenio, The role of non-equilibrium vibrational structures in electronic coherence and recoherence in pigment-protein complexes, *Nat. Phys.* **9**, 113 (2013).
- [50] P. K. Mogensen and A. N. Riseth, Optim: A mathematical optimization package for Julia, *J. Open Source Softw.* **3**, 615 (2018).
- [51] Z. H. Zhan, J. Zhang, Y. Li, and H. S. Chung, Adaptive particle swarm optimization, *IEEE Trans. Syst. Man Cy. B* **39**, 1362 (2009).
- [52] V. Chorošajev, T. Marčiulionis, and D. Abramavičius, Temporal dynamics of excitonic states with nonlinear electron-vibrational coupling, *J. Chem. Phys.* **147**, 074114 (2017).
- [53] D. Abramavičius and L. Valkunas, Geminant pair recombination in molecular systems with correlated disorder, *Phys. Rev. B* **68**, 245203 (2003).
- [54] A. Eisfeld, S. M. Vlamings, V. A. Malyshev, and J. Knoester, Excitons in Molecular Aggregates with Lévy-Type Disorder: Anomalous Localization and Exchange Broadening of Optical Spectra, *Phys. Rev. Lett.* **105**, 137402 (2010).
- [55] O. Rancova, M. Jakučionis, L. Valkunas, and D. Abramavičius, Origin of non-Gaussian site energy disorder in molecular aggregates, *Chem. Phys. Lett.* **674**, 120 (2017).